Tectonophysics 693 (2016) 453–464

Contents lists available at ScienceDirect

Tectonophysics

journal homepage: www.elsevier.com/locate/tecto

Structure and kinematics of the Sumatran Fault System in North Sumatra (Indonesia)

David Fernández-Blanco [a,*], Melody Philippon [b], Christoph von Hagke [c]

[a] Institut de Physique du Globe de Paris, Sorbonne Paris Cité, Univ Paris Diderot, CNRS, F-75005 Paris, France
[b] UMR CNRS 5243, Géosciences Montpellier, Université des Antilles, Campus de Fouillole, 97100 Pointe à Pitre, French West Indies
[c] RWTH Aachen University, Institute of Structural Geology, Tectonics and Geomechanics, Lochnerstraße 4-20, 52056 Aachen, Germany

ARTICLE INFO

Article history:
Received 28 September 2015
Received in revised form 8 April 2016
Accepted 27 April 2016
Available online 10 May 2016

Keywords:
Strike-slip system
Slip partitioning
Forearc sliver plate
Sumatran Fault System
Sumatra

ABSTRACT

Lithospheric-scale faults related to oblique subduction are responsible for some of the most hazardous earthquakes reported worldwide. The mega-thrust in the Sunda sector of the Sumatran oblique subduction has been intensively studied, especially after the infamous 2004 Mw 9.1 earthquake, but its onshore kinematic complement within the Sumatran subduction, the transform Sumatran Fault System, has received considerably less attention. In this paper, we apply a combination of analysis of Digital Elevation Models (ASTER GDEM) and field evidence to resolve the kinematics of the leading edge of deformation of the northern sector of the Sumatran Fault System. To this end, we mapped the northernmost tip of Sumatra, including the islands to the northwest, between 4.5°N and 6°N. Here, major topographic highs are related to different faults. Using field evidence and our GDEM structural mapping, we can show that in the area where the fault bifurcates into two fault strands, two independent kinematic regimes evolve, both consistent with the large-scale framework of the Sumatran Fault System. Whereas the eastern branch is a classic Riedel system, the western branch features a fold-and-thrust belt. The latter contractional feature accommodated significant amounts (c. 20%) of shortening of the system in the study area. Our field observations of the tip of the NSFS match a strain pattern with a western contractional domain (Pulau Weh thrust splay) and an eastern extensional domain (Pulau Aceh Riedel system), which are together characteristic of the tip of a propagating strike-slip fault, from a mechanical viewpoint. For the first time, we describe the strain partitioning resulting from the propagation of the NSFS in Sumatra mainland. Our study helps understanding complex kinematics of an evolving strike-slip system, and stresses the importance of field studies in addition to remote sensing and geophysical studies.

1. Introduction

Lithospheric-scale strike-slip faults develop worldwide by slip partitioning during oblique convergence between two tectonic plates. These trench-parallel strike-slip faults accommodate margin-parallel slip while the corresponding slabs subduct with slip normal to the margin. As a result, individual slivers of lithosphere (sliver plates) develop in the upper plate between the trench and its associated strike-slip faults (e.g. Fitch, 1972; Karig, 1978) (Fig. 1, panel A and B). These faults, reaching hundreds of kilometers of cumulative displacements along thousands of kilometers, favor localization of magmatic intrusions and influence the position of the volcanic arc (Sieh, 1988). Sense and rate of motion along these faults can be quantified using geophysical data, and large-scale domains of compression and tension can be identified in relation to the degree of convergent and divergent slip resulting from fault geometry (Prescott, 1981; Sieh, 1988).

The Peru-Chile trench and the Atacama fault in the west coast of South America (e.g. Allen, 1965), the Nankai Trough and the Median tectonic line in Japan (e.g. Kaneko, 1966), and the Sunda trench and the Sumatran Fault System in Sumatra Island (e.g. Katili, 1970; Fitch, 1972) are prominent examples of this particular tectonic setting highly prone to large, hazardous earthquakes. The system associated with the Sumatran Fault System (SFS) (Fig. 1.A) has attracted researchers, especially after the infamous 2004 Mw 9.1 earthquake off the west coast of northern Sumatra (Subarya et al., 2006; Fu and Sun, 2006; Chlieh et al., 2007; Franke et al., 2008). Intensive geophysical studies provide a good understanding of seismic coupling and vertical motions along the forearc side of the sliver plate (Simoes et al., 2004; Natawidjaja et al., 2004, 2006; Sieh, 2007; Berglar et al., 2010; Collings et al., 2012; Cook et al., 2014; Martin et al., 2014; Frederik et al., 2015). However, structural and kinematic analyses in the SFS and derived structures need to be improved to help evaluate the seismic hazard potential, and thus mitigate the impact of the devastating earthquakes associated with this system (e.g. Ishii et al., 2005; Moreno et al., 2010).

Sieh and Natawidjaja (2000) studied different sectors of the SFS using photo-interpretation in an area ranging from 6.75°S to 4.4°N;

* Corresponding author.

http://dx.doi.org/10.1016/j.tecto.2016.04.050
0040-1951/

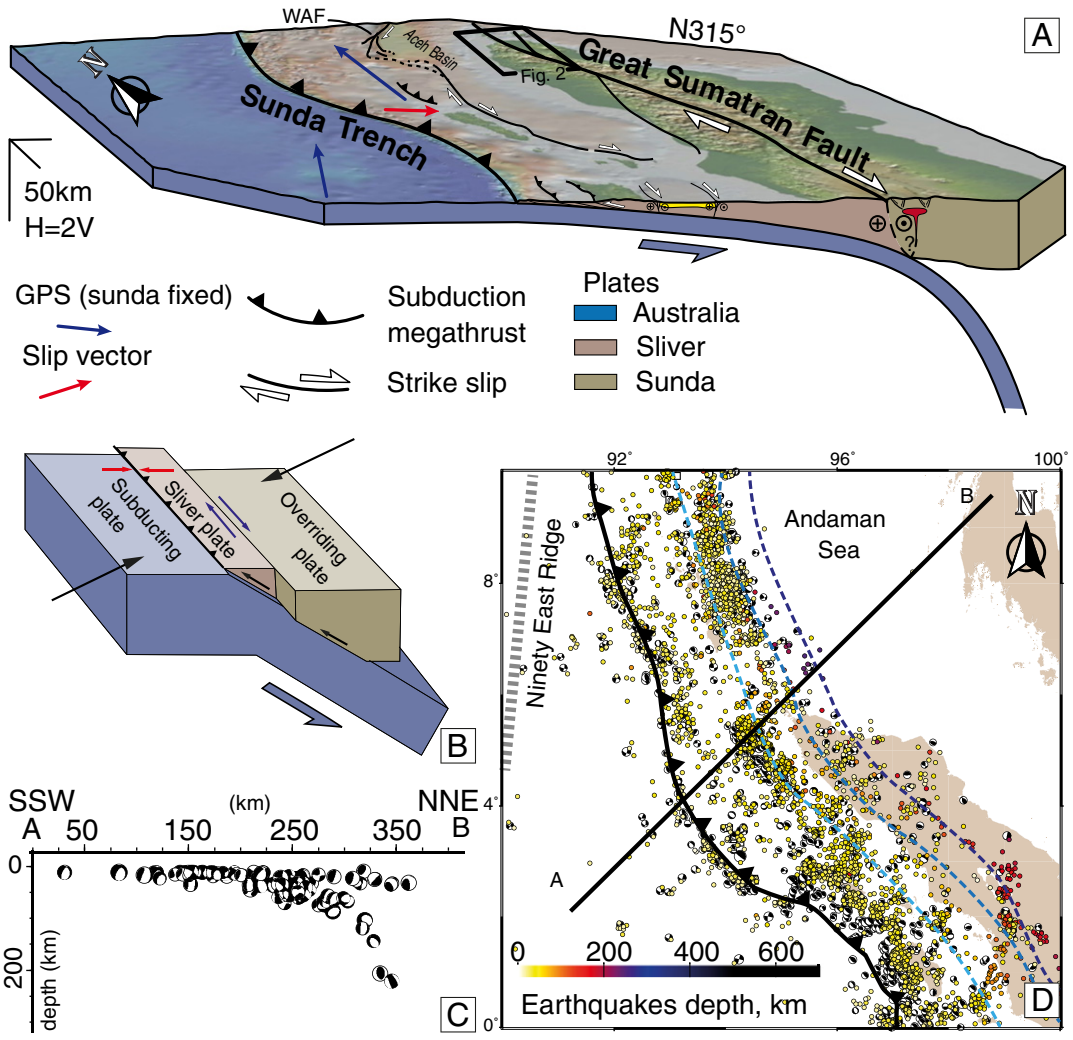

Fig. 1. General tectonic context in the Sumatran section of the Sunda forearc. A: Real-scale 3D view of the tectonic configuration of the northern sector of the Sumatran section of the Sunda arc, showing the main regional and tectonic-scale features, as well as GPS and slip vectors. The frontal cross-section transects the Nias island and the Toba caldera in a direction roughly perpendicular to the Sunda Trench and the Sumatran Fault System. Location of the study area (frame of Fig. 2) is also shown. Northern Sumatra off-shore structures are from Martin et al. (2014); WAF stands for West Andaman Fault. B: Idealized block diagram showing the geometry of the sliver plate and overall motions under oblique subduction (modified from McCaffrey (2009) to emphasize correlations with panel A). Cross-section (C) and map view (D) showing the location and depth of earthquakes and their focal mechanisms in the study area and surroundings, after Heuret and Lallemand, (2005). Blue dotted lines represents the slab 50 km-isocontours with a color gradient from light to dark with increasing depth (Gudmundsson and Sambridge, 1998).

we study the geometry of the northern sector of Sumatra including the islands in northwest offshore Sumatra, which have not been described in detail in previous studies. Here, we investigate whether the structural framework of the northern sector of the Sumatran Fault System (NSFS) is variable, and how this variability might reflect strain partitioning. To this end, we analyze new detailed structural data from the NSFS, with special attention to the aforementioned islands. These islands exhibit the youngest deformation in relation to oblique convergence, located at the leading edge of northwestwardly propagating continental sliver deformation exposed on land (Jarrard, 1986; McCaffrey, 1991, 1992).

2. Present day geodynamic context

2.1. Geometry, kinematics, volcanism and seismicity

The strike-slip SFS accommodates the high-angle oblique subduction of the Australian Plate below the Sunda Plate. The right-lateral transpressional SFS runs parallel to the trench with an overall linear, slightly sinusoidal geometry (e.g. Natawidjaja, 2002), and cuts the Sumatran lithosphere vertically down to the asthenosphere (Bellier and Sébrier, 1994). The SFS defines the eastern boundary of the Sumatran sliver plate; its western limit is the NNW–SSE curved Sunda Trench (Fitch, 1972; Karig, 1978; McCaffrey, 2009) (Fig. 1.A). This sliver plate thus represents an individualized sector of the Sunda Plate forearc (more than 1650 km long and 250–300 km wide), which moves northwestwards along the trench, driven by basal shear (McCaffrey et al., 2000; McCaffrey, 2009) (Fig. 1.B).

The Australian Plate moves northwards at a rate of 59 ± 3 mm year^{-1} at the latitude of Sumatra Island, east of the Ninety East ridge; west of the ridge, the Indian Plate moves at a lower rate of 39 ± 3 mm year^{-1} (Martin et al., 2014). Both, the Australian and Indian plates move almost parallel to the N-S trending Sunda Trench. The Sunda Trench shows pure dip slip motion at a mean rate of 45 mm year^{-1}, accommodating the normal-to-trench motion of Australia (Jarrard, 1986; McCaffrey, 1991, 1992; Bock et al., 2003). The movement parallel to the trench is partly (~2/3) accommodated by strike-slip along the SFS at rate of 24.5 ± 4.5 mm year^{-1} (Chlieh et al., 2008), and partly (~1/3) by full margin parallel motion probably between the forearc islands and the trench (McCaffrey et al., 2000) (Fig. 1.A). Slip rates increase towards the northwest along the SFS, as indicated by the arcuate shape of the subduction trench, a distant pole of rotation, and earthquake slip vectors from the subduction mega-thrust, as well as GPS data (Huchon

and LePichon, 1984; McCaffrey, 1991). Strain partitioning into dip-slip and strike-slip components is largest in northernmost Sumatra, due to the increasing obliquity between the orientation of the subduction trench and absolute plate motions.

The SFS transects Sumatra Island in its entirety and largely controls the tectonic architecture of the island (McCaffrey, 1991; Genrich et al., 2000; Simons et al., 1999, 2007; Bock et al., 2003; Socquet et al., 2006), which is prone to frequent volcanic eruptions and high magnitude earthquakes (e.g. Ninkovich et al., 1978; Walter and Amelung, 2007; Chlieh et al., 2008) (Fig. 1, panels C and D). The volcanic arc in Sumatra Island runs parallel to the subduction zone and sidewise with the SFS, above the 100–150 km depth contours of the subducting plate (Pesicek et al., 2008; Hatherton and Dickinson, 1969; Sieh and Natawidjaja, 2000). The mechanically weaker behavior along the magmatic arc concentrates deformation and ultimately influences the position of the SFS, which in turn favors the location of volcanic centers within major releasing stepovers, while controlling the morphology of the volcanoes (Jarrard, 1986; McCaffrey, 1992; Bellier and Sébrier, 1994).

Locally, the SFS shows changes in strike resulting in tens of potentially-seismic faults defining releasing and restraining bends, that are several kilometers wide (Natawidjaja, 2002; Kasmolan et al., 2010). Such fault stepovers localize deformation and reduce the potential area of slip per seismic event. This leads to observed earthquake magnitudes of Mw 7.5 or smaller along the entire fault (McCaffrey, 1992). This local segmentation along the SFS leads to internal deformation in the forearc sliver plate (Katili and Hehuwat, 1967; Bellier and Sébrier, 1994; Prawirodirdjo et al., 2000; Sieh and Natawidjaja, 2000) (Fig. 1.D).

2.2. Geology of Northern Sumatra

Northwards of ~5.05°N, the SFS accommodates motion along two fault strands that diverge at a ~30° angle, creating two topographic highs and confining a topographic low in between (Fig. 2). For descriptive simplicity, we term these features as the eastern and western branches of the Northern sector of the Sumatran Fault System (NSFS) and the onshore basin, respectively. The motion along the branches of the NSFS readily controls the development of the topography bounding the onshore basin. Whereas the eastern branch transects basement igneous rocks and Miocene and Quaternary volcanic and sedimentary rocks, the western branch almost exclusively cuts basement igneous rocks (Fig. 2). This lithological contrast might be contributing to the different topographic heights between both branches; topography in the eastern branch of the NSFS is significantly lower than in the western branch, although the former encloses magmatic additions by at least two volcanic centers. The flat morphology of the onshore basin is controlled by the meandering dynamics of the Aceh river, flowing from the mountain highs in the south to the Andaman Sea, as the basin gains width, up to a maximum of ~35 km at the coast. Both fault branches run straight for at least ~80 km before reaching the northernmost coast of Sumatra, and continue farther northwest, running parallel to each other, off the coast of north Sumatra Island. Near the coast in the Andaman Sea, several islands develop in relation to each branch of the NSFS; the eastern branch runs through the Pulau Weh Island in the northernmost sector of the study area, while the western branch marks the eastern boundary of the Pulau Aceh archipelago in the westernmost sector of the study area (Fig. 2). Farther north, the NSFS transforms into the Andaman spreading center at its northwestern terminus (Curray et al., 1979).

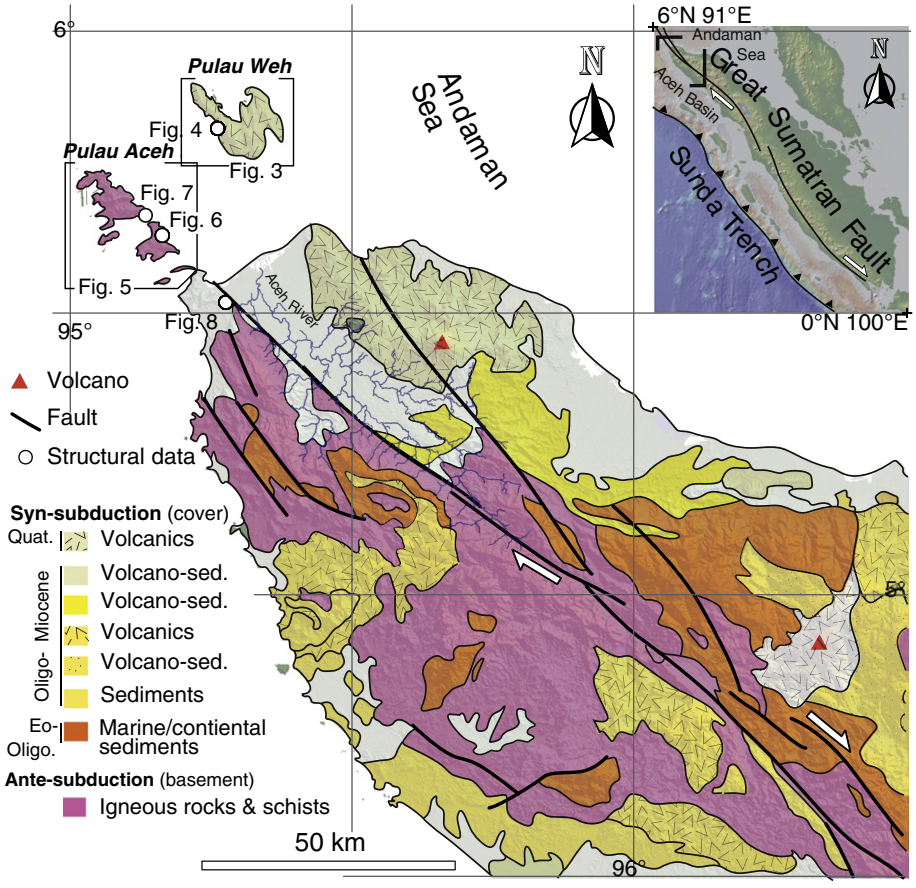

Fig. 2. Simplified geologic map of the study area and surroundings (on top of the ASTER GDEM 1-arc), showing the main cover units (syn-subduction) on top of basement (ante-subduction). Location of the areas used during the DEM analyses, and that of the outcrops discussed in this contribution, and their corresponding figures, are also indicated.

3. Structural analysis of Digital Elevation Models (DEMs) and in the field

We combined Digital Elevation Model (DEM) analysis and outcrop structural data in order to better define the geometry and kinematics of the NSFS. We performed structural interpretation of DEMs with a horizontal resolution of 30 m, derived from the Advanced Spaceborne Thermal mission and Reflection Radiometer (ASTER GDEM) using the FaultTrace module of TerraMath WinGeol (TerraMath®). The FaultTrace tool uses the three point geometrical method of planar attributes in order to identify geological structures; the intersection line produced by the contact between topography and a geological planar feature (such as bedding or fault surfaces) is defined by at least three points, in turn characterizing the dip and dip direction of the geological object. To this end, the FaultTrace tool computes the best-fit plane defined by manually picked input points on the intersecting line. One relevant advantage of this tool is the ability to visually adjust the geological planes during mapping, thus constraining the most representative orientations. The error range is about ~10° for dip direction and ~5° for dip angle, thus slightly higher, but comparable to the uncertainties of field data acquisition (Reif et al., 2011). ASTER GDEM resolution is well suited for geometrical analysis of the topography to capture the main regional structures, but outcrop scale structures are not resolved. To produce better outcomes, we built our tectonic models focusing on the analysis of large-scale features and discarding numerous smaller, potentially ambiguous structures visible in the DEM. Similarly, to avoid confusion and map clustering, we have deliberately removed planar features that were observed too close to each other but provided the same information; in these cases, only the most representative, and often more pronounced, planar feature was plotted.

Additionally to our DEM analysis, we checked results in a field campaign with focus on outcrop-scale structural and kinematic analyses along the NSFS (Fig. 2). As no constraints on absolute timing of deformation exist for the area, we are only able to establish a relative chronology of deformation.

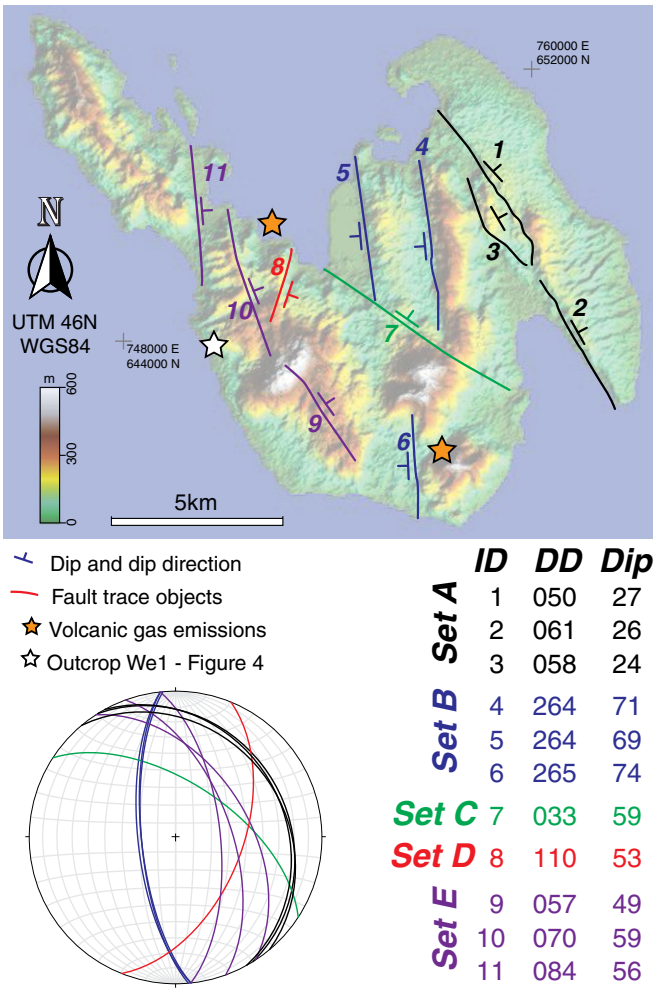

Fig. 3. GDEM analysis of the Pulau Weh Island. On the left hand side is the topographic map of Pulau Weh and the structural features mapped with the FaultTrace module of TerraMath WinGeol (TerraMath®). Dip azimuth and dip angle are represented in map view at the top, and their values shown in table form, in the bottom right of the figure. Stereoplot representation of such features is at the bottom left. Colors indicate different sets. A white star indicates the location of the Outcrop We1 (Fig. 4). Orange stars are used to locate areas with gas emission in relation to volcanic activity.

4. Geometry of the NSFS

We investigate the geometry of the NSFS at the northern end of Sumatra and at its northernmost offshore islands, i.e., between 4.5°N and 6°N latitude. We thus cover the fault from the location where it bifurcates as it propagates towards the northwest (Jarrard, 1986; McCaffrey, 1991, 1992), as well as the areas where the leading edge of deformation is exposed on land (Fig. 2 for location).

4.1. Pulau Weh Island and NSFS eastern branch

Pulau Weh Island is located in the northeast offshore prolongation of Sumatra Island at the eastern splay of the NSFS (Fig. 2). Peninsulas trending NNW–SSE (i.e. parallel to the regional trend of the NSFS) control the shape of the Pulau Weh Island. Likewise, the first-order morphology of the island shows continuous topographic highs, indicating close relation to the NSFS. Our detailed topographic analysis reveals a minimum of eleven planar large-scale features (several kilometers in length) cutting the island (Fig. 3). These large-scale features can be bedding surfaces, faults or fractures. We classified these planar objects by analysis of their extension, shape, strike and dip, and pooled them into distinct sets. At least three different predominant sets of large-scale structures can be distinguished on the basis of strike and dip (Fig. 3). Lateral continuation and predominant occurrence of planar features, marking most of the morphological highs in the island, suggest that these sets are related to faults rather than bedding.

A first set of large structures observed in the eastern part of the island follows the main direction of the NSFS. Determined dip directions are constant towards the northeast with values of approximately 25° (Set A, black great circles in Fig. 3). The second cluster contains regional features that dip towards the west at angles of ~70–75° (Set B, blue great circles in Fig. 3). The maximum dip line of Set B is perpendicular to that of Set A. In the central region of the island, Set B bounds two pronounced ridges in the north and part of two topographic highs in the south. Additionally, smaller structures distributed across the entire island seem to follow the same trend. A third structure crosscuts the island in its central part, striking NW-SE, and dipping at ~60° towards the northeast (Set C, green great circle in Fig. 3). Farther west, a feature striking NNE–SSW, and dipping at ~55° towards the ESE, can be detected (Set D, Fig. 3, red great circle). Similarly to Set C, we note that the trend of Set D is observable across the entire island in local spots, but it is difficult to confidently interpret these smaller features. Finally, heading west, the strike direction of Set E resembles that of the NSFS in the south of the island and slightly rotates towards the NNE in its north. Similarly, dips progressively change from 50° to 65° towards the northwest (Set E, purple great circles, Fig. 3).

4.1.1. Outcrop We1–5°49′39.92″N; 95°15′41.39″E

Exposure, as well as access to most sectors of Pulau Weh Island, is very limited. However, at one spot at the central west coast, structures are well exposed at the scale of tens of meters, due to a relatively fresh

road cut, allowing for multiple measurements of fault and bedding planes (Fig. 4).

A set of faults crosscuts the entire outcrop. Several fault planes are exposed, consistently dipping steeply towards the ESE. The single kinematic indicator found suggests top-to-the-southeast movement (Fig. 4). Bedding offset is not observed along this fault or any other, indicating that this normal component is not accommodating much strain. In the southeastern part of the outcrop, bedding surfaces constantly dip at an angle of approximately 50° towards the northeast. Going farther to the northwest, beds dip at 70° towards SSE. The cross-cutting relationship between the two different plane sets is not exposed. However, the beds dipping 190/70 form the southern limb of an upright similar fold, with its fold axis plunging at 20° towards the west. This structure is cut by a fault dipping at 38° towards the northeast. No kinematic indicators were found on this fault.

4.2. Pulau Aceh Archipelago and NSFS western branch

Pulau Aceh is an archipelago composed of five curved-shaped islands located offshore northernmost Sumatra (Fig. 2), to the west of Pulau Weh Island. The eastern end of the Pulau Aceh Archipelago defines a sharp straight line trending NNW–SSE that coincides with the expected offshore prolongation of the western branch of the NSFS (Fig. 5).

The planar structures shown in Fig. 5 are the most prominent features, extending often along entire islands in E-W direction. Based on their orientation, we distinguished three major sets of structures among a total of 23 planar features (Fig. 5). Features of Set 1 strike ENE, have limited length (1–2 km along strike) and often appear in clusters, with planes characterized by periodic spacing (200 to 300 m). At archipelago scale, Set 1 planes dip roughly north, and have dip values progressively increasing from subhorizontal to ~50° towards the south (Set 1, black great circles in Fig. 5). Set 2 consists of roughly S-dipping ENE-trending features that crosscut at occasions the whole length of the islands. Set 2 dip values progressively decrease southward, from 45° to subhorizontal (Set 2, blue great circles in Fig. 5). At the scale of the whole archipelago the strike of Set 1 and Set 2 are similar, while their dips display a roughly constant angular relation of ~45°. Set 3 is characterized by two opposite-dipping structures striking NNW with dip values of 60° that crosscut the two aforementioned planar sets of mappable structures (Set 3, red great circles, Fig. 5).

Structures in Set 1 are interpreted as regional bedding, given their limited lateral continuation, and periodical spatial distribution. Straight appearance and continuity over many kilometers allow interpretation of Set 2 and Set 3 as faults, shallow and steeply dipping, respectively. Heading to the southeast, dip values consistently increase for the regional bedding (Set 1) and decrease for the shallow dipping faults (Set 2), maintaining an angular relation of roughly 45° between both sets. This angular relation suggests that the shallow dipping faults affected consistently dipping regional beds. These faults were later rotated, reaching 45° at their northwest extent, leading in turn the variation in the bedding dips. Set 3 corresponds to younger steeply dipping fault planes crosscutting both the bedding and the shallow dipping fault set.

4.2.1. Outcrop Ac1–5°38′17.10″N; 95°09′51.06″E

Outcrop Ac1 is located in Pulau Nasi, one of the southern islands of Pulau Aceh Archipelago (Fig. 5 for location). Outcrop Ac1 reveals an

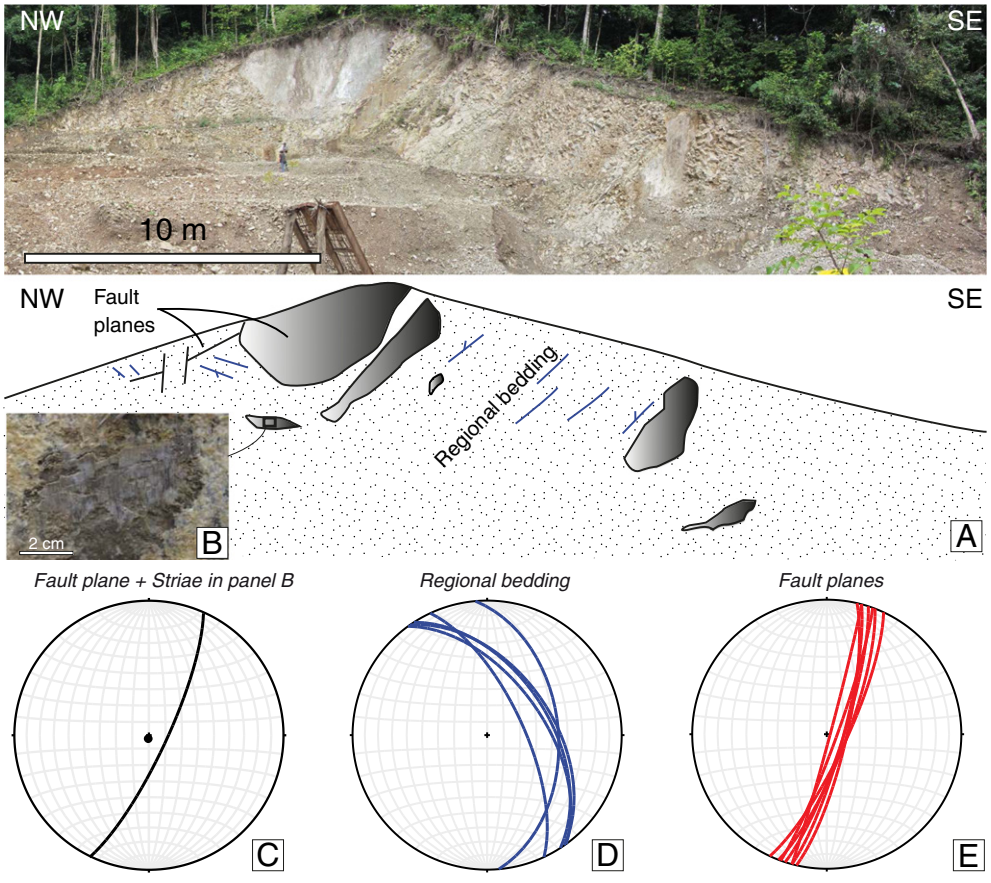

Fig. 4. Outcrop We1. A: Top image shows a panoramic picture of the outcrop, and its interpretation is at the bottom. Panel B is a close up of fault-related calcite and its striae. To the right, stereoplots of (C) the great circle for the fault plane and its striae in panel B, and great circles of (D) regional bedding (in blue) and of (E) main fault planes (in red).

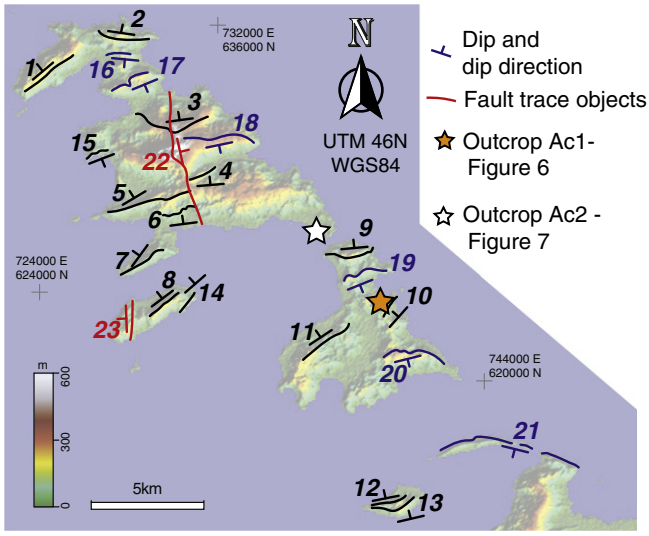

	ID	DD	Dip
Set 1	1	323	12
	2	013	27
	3	352	26
	4	356	23
	5	334	13
	6	350	14
	7	303	07
	8	329	05
	9	354	31
	10	313	44
	11	329	37
	12	345	50
	13	339	22
	14	316	01
	15	156	02
Set 2	16	183	46
	17	154	13
	18	168	22
	19	159	12
	20	164	11
	21	190	01
Set 3	22	076	55
	23	273	60

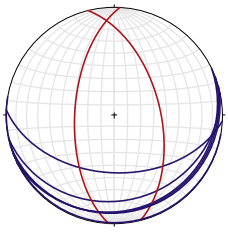

Fig. 5. GDEM analysis of the Pulau Aceh Archipelago. On the left hand side is the topographic map of the Pulau Aceh Archipelago and the structural features mapped with the FaultTrace module of TerraMath WinGeol (TerraMath®). Dip azimuth and dip angle are represented in map view and their values shown in table form, at the right hand of the figure. Stereoplot representation of such features is between the aforementioned panels. Colors indicate different sets of faults; beds are not shown. Orange and white stars indicate the location of the outcrop Ac1 and Ac2, respectively.

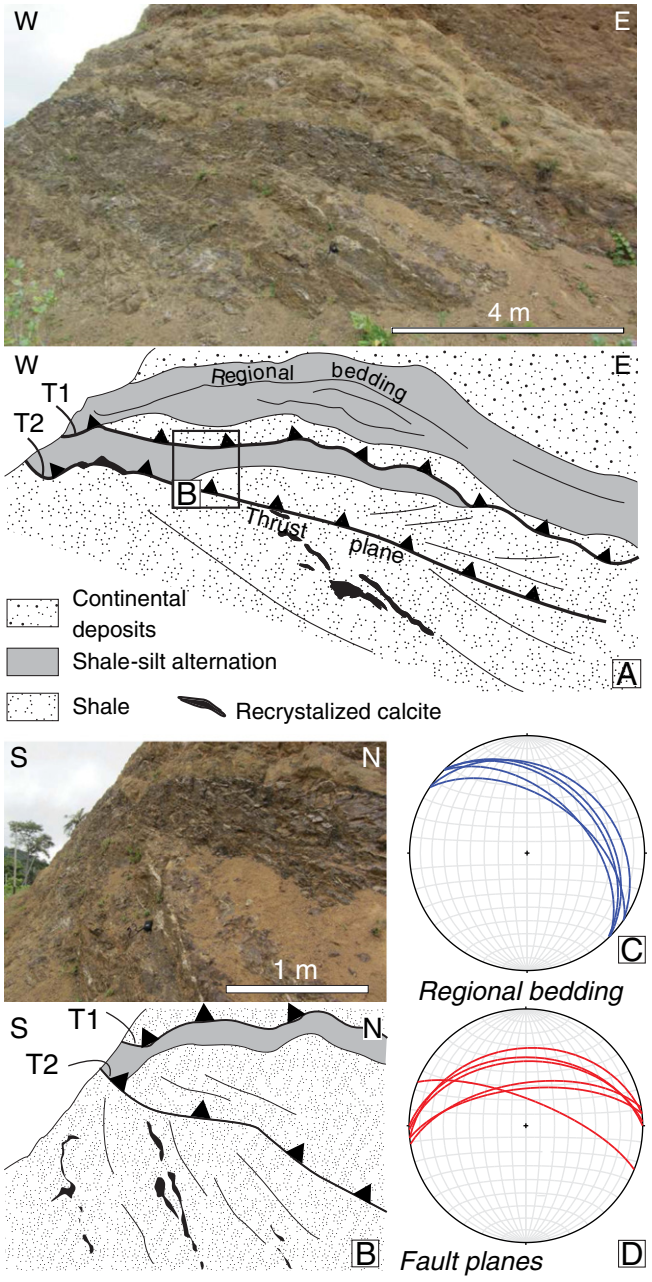

Fig. 6. Outcrop Ac1. Panel A: Upper side shows a panoramic picture of the outcrop, with its interpretation bellow. Panel A is oriented roughly E-W, i.e. parallel to the thrust planes. Panel B: Close ups. Upper side shows calcite-filled veins parallel to the bedding, and bellow its schematic interpretation. Panel B is oriented roughly N-S, i.e. perpendicular to the thrust planes. Panel C and D: Stereoplots, with great circles for the regional bedding (in blue) and the shallow dipping faults (in red).

almost complete 3D exposure of a stratigraphic sequence, transected by low angle reverse faults.

Outcrop Ac1 (Fig. 6) shows a shallowing upwards stratigraphic sequence. From bottom to top: (*i*) deep-water black shales, (*ii*) silt-shale alternations, and (*iii*) pluri-decametric channels filled with fluvial red sands and conglomerates. Northeastwards dipping regional bedding (~40°) is transected by faults dipping north from ~40° to ~60°. The faults are located in the shales at the base the sequence and in the interlayered silt and shale levels. Often, fault planes filled with recrystallized cm-thick calcite are parallel or subparallel to bedding. A mesoscale fault-propagation-fold (tens of meters) is identified by the geometry of the transition from dark shales to lighter-colored silts in relation to a thrust plane (T1 in Fig. 6, panel A). Close to a W-E directed profile drawn by the topography, this stratigraphic contact hits the thrust plane at a low angle (upper left side of panel A). The same relation is observed on the other side of this three-dimensional exposure (a N-S directed profile), where this fault-bend fold is located above another thrust surface (T2 in Fig. 6 panel A and B).

4.2.2. Outcrop Ac2–5°40′12.77″N; 95°07′56.87″E

Outcrop Ac2 is located in Pulau Breueh, one of the northern islands of Pulau Aceh Archipelago (Fig. 5 for location), and it exposes a deformed sedimentary series.

Outcrop Ac2 displays a series of interlayered sandstones and siltstones affected by folds and faults. Regional bedding trend N50—N90°, dip 40° towards the SSE, and is often affected by low-amplitude folding. The axial plane of this folding is vertical and strikes NNW–SSE ([D] in Fig. 7). We identified two distinct sets of features that cross-cut bedding

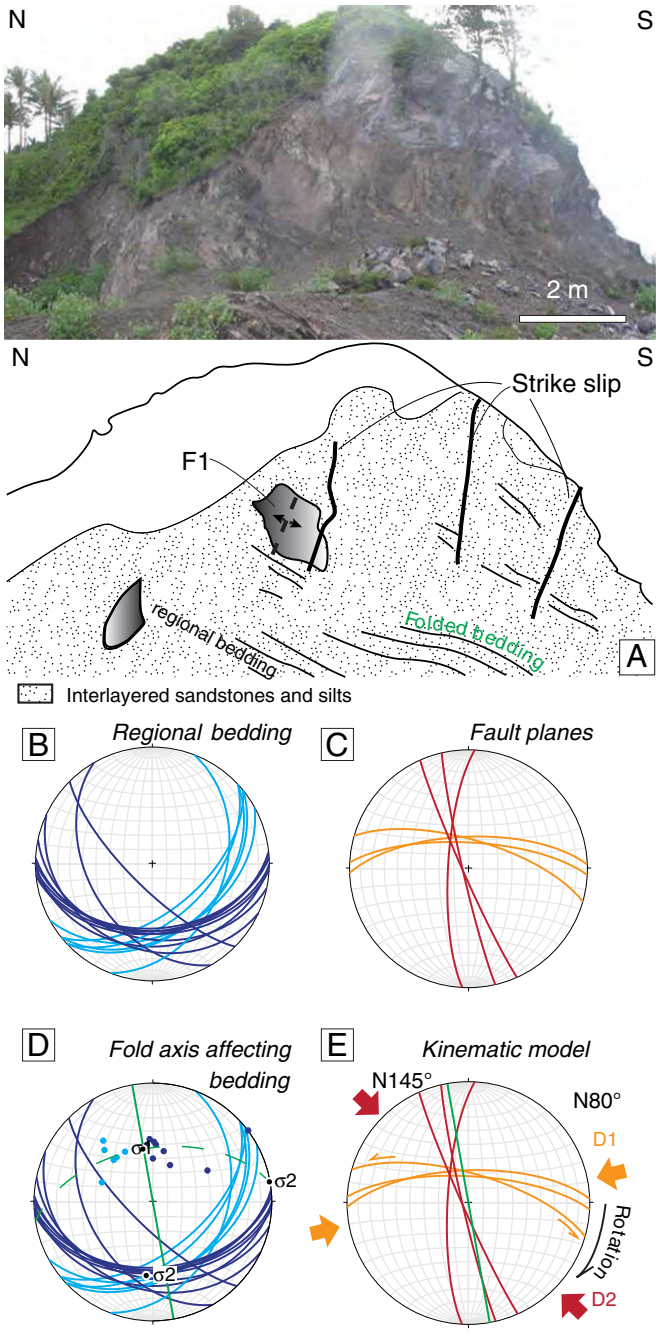

Fig. 7. Outcrop Ac2. Panel A: Upper side shows a panoramic picture of the outcrop and below its interpretation. At bottom, stereoplots showing: [B] the great circles for the regional bedding (in two types of blue); [C] steeply dipping faults (in orange and red); [D] fold axial plane of the low-amplitude folds (in green); and [E] schematic kinematic model of stress field rotation.

without obvious vertical displacement, both with subvertical dips; (*i*) one set trending N-S and dipping west ([C, red] in Fig. 7), and (*ii*) another set oriented E-W and dipping to the north ([C, orange] in Fig. 7). The E-W set represent fault planes in two locations in the outcrop, which are crosscut by the N-S striking system and gently folded (F1 in Fig. 7). This structural setting fits well in a strike-slip setting.

4.2.3. Outcrop Su1–5°31′08.35″N; 95°16′34.41″E

Outcrop Su1 is located on Sumatra mainland near the northern coast and exposes a large continuous fault plane trending roughly NW-SE. The fault outcrops in a quarry and is aligned with the eastern boundary of the Pulau Aceh Archipelago (Fig. 2 for location).

Outcrop Su1 exhibits an excellent exposure of the western branch of the NSFS fault plane, with numerous well-preserved kinematic indicators (Fig. 8). The fault plane dominating the outcrop, roughly spanning an exhumed area of ~450 m^2, trends ESE-WNW and consistently dips at 54° to the SSW. This fault has a dextral-normal sense of movement, as shown by numerous striae and calcite recrystallizations with kinematic indications that systematically indicate top-to-the-W motion and oblique slip plunging at 40° (see Fig. 8). Around 30 m to the SE, another large fault plane is roughly oriented N-S and dips at ~80° towards the west. Between these two systems a series of steeply dipping faults with no apparent vertical displacement deform the rocks into a tectonic breccia. Bedding dips gently to the west at the southeastern side of the outcrop, and becomes vertical near the main fault plane.

5. Structure and kinematics of the NSFS

5.1. Interpretation of the observations in the outcrops

We interpret the faults exposed in Outcrop We1, with very steep dip and lack of significant vertical offset, as a strike-slip fault system, for two main reasons; the spacing among the fault planes is irregular and they often appear in tight clusters, without branching out/coalescence among planes, and overall resembles a broad area of a strike-slip corridor, in opposition to a "domino-like" normal fault system. Furthermore, besides the presence of just one kinematic indicator, we tentatively allocate Outcrop We1 in relation to either Set D or Set E of our DEM analysis. The former interpretation is based on the coincidence in trend between the outcrop and Set D. The latter interpretation is based on coincidence in location: Set E is geographically closer to the outcrop, which is in a southward position from Set E ID 11 and almost coincidental with its trend (if extrapolated linearly south).

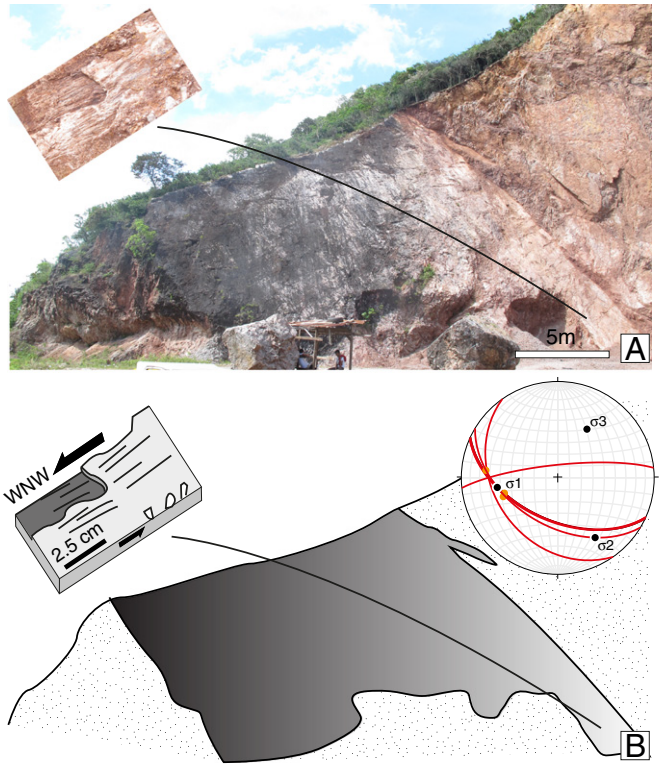

Fig. 8. Outcrop Su1. Field picture [A] and its interpretation [B]. Inset shows a close up of the fault plane, with top-to-the-W strikeslip kinematic indicators. The stereoplot shows several fault plane measurements and associated striae as well as the principal stress axes.

We interpret Outcrop Ac1 as the result of thrust activity. This interpretation can explain the shallowing-upwards stratigraphic sequence as the result of regional thrust-related uplift (leading to a tectonically induced regression), and the presence of the local thrusts and related folds that duplicate the stratigraphy. In the absence of clearer kinematic indicators, i.e. striae, we infer northward thrust movement on the basis of the geometry of the anticline at the hanging wall of T1 thrust plane. Strain is localized in the shale layers, where bedding parallel shear and calcite recrystallization is observed.

Outcrop Ac2 observations are symptomatic of strike-slip motion for the E-W set, even in the absence of kinematic indicators. Similarly, outcrop location and irregular distribution of the N-S striking set suggests an strike-slip origin, although the absence of a clear fault plane exposure cannot completely overrule their formation as shear joints. From the orientation of fold axial planes we deduce an ENE-WSW trend for the principal stress axis ($\sigma 1$). This ENE-WSW direction of $\sigma 1$ is also compatible with a left lateral motion along the E-W strike-slip. We thus suggest that folding is coeval with sinistral E-W strike-slip, and is the result of a single deformation event. Similarly, we consider that the uniform spatial distribution of tilted regional beds and their consistency with fold orientation are indicative of the development of both features as part of the aforementioned deformation event. Strain analysis based on assumed ideal stresses needed to develop the geometry of both features, when taken together suggests they developed under an ENE-WSW $\sigma 1$ (D1, stereoplot [E], Fig. 7). Later, a second deformation event leads to the development of N-S strike-slip, transecting the previously formed features, as inferred by the crosscutting relations (D2, stereoplot [E], Fig. 7). This later event suggests a clockwise rotation of the stress field from ENE-WSW to NW-SE ([E] in Fig. 7).

We interpret Outcrop Su1 as a large scale negative flower structure within the NSFS at this location. This interpretation is based on the dextral transtensive kinematics of the dominating fault and the opposite dipping of the other major fault, taken together with the apparent lack of vertical displacement on the minor fault planes, and their orientation in coupling with the folding of bedding towards them. The overall configuration of Outcrop Su1 shows that strain may be distributed along the strike of the fault, and the damage zone related to the active fault may reach substantial widths. Furthermore, this kinematic setting, despite fitting the overall framework, is different from the observations on Pulau Aceh and Pulau Weh islands. This differences indicate variability of kinematics of the NSFS within small distances, and stresses the need for detailed analysis of the respective subsystems.

5.2. The Pulau Weh Riedel system

The observed structures, taken together with the tectonic strike-slip framework of the Pulau Weh Island and its geographic location, atop of the eastern fault branch of the NSFS, allow us to interpret it as a Riedel system (Fig. 9). Indeed the strike directions of observed large-scale structures fit remarkably well with strike directions within a Riedel system. However, additional complexity is revealed when taking into account dip variations. Analysis of the different topographic features allows for pooling determined structures into distinct sets of mappable structures. The most prominent set (Set A), which dominates the morphology of the entire island, is parallel to the NSFS. In a Riedel framework, it corresponds to the main direction of imposed shear, oriented at a 45° angle from the maximum compressive stress (Fig. 9). Set B, which is oriented at an angle of approximately 15° to the direction of Set A correlates to R-shears, while Set C corresponds to P-shears. Even though R-shears are not apparent in our DEM analysis, several small scale features, especially in the southernmost part of the island, could be interpreted as such. We note that Set E changes strike and dip direction from east to west. We interpret this as a local particularity, i.e. as variations within the main direction of fault strike with respect to $\sigma 1$. Our outcrop analysis on Sumatra Island showed that such variations can be reasonably expected within the overall framework. This is

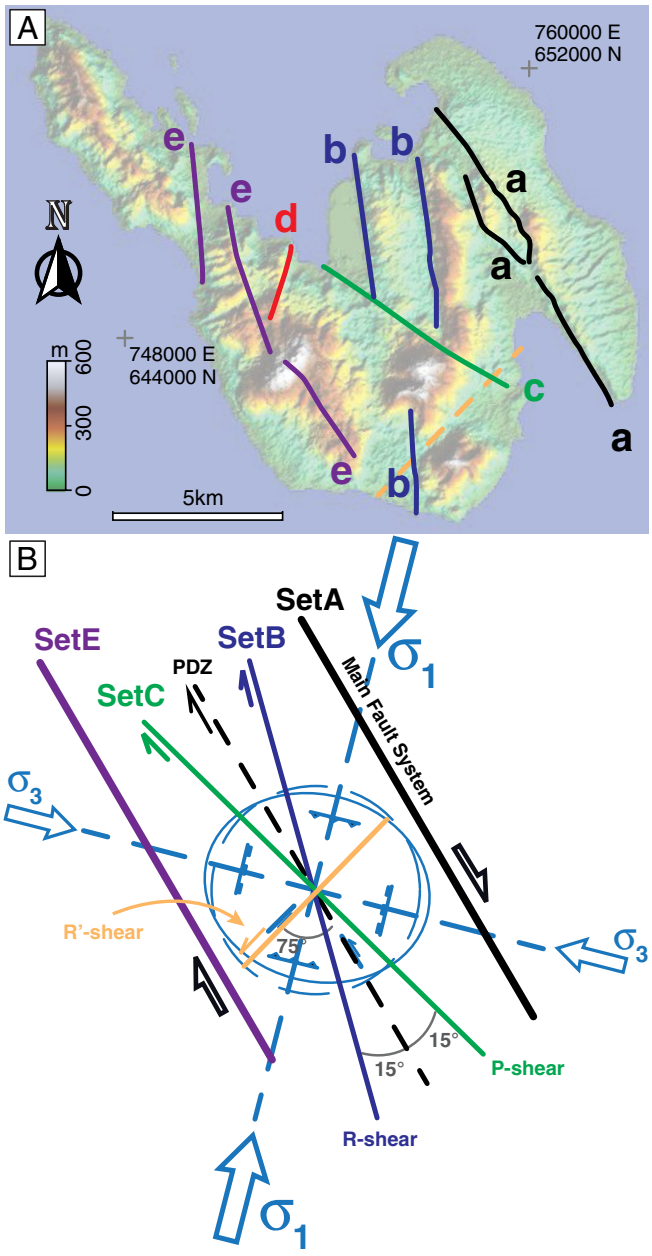

Fig. 9. Structural interpretation in Pulau Weh: Riedel system.

corroborated by complex topography and highest peaks on the island, which may be the result of a positive flower structure in this area. Consequently, we interpret Set D as R-Shears with respect to Set E. Likewise outcrop We1 fits in the overall Riedel system, and corresponds to local variation of Set E, that is the main direction of imposed shear.

Dip of the respective systems and limited knowledge on their kinematics complicate this straightforward interpretation. Particularly, due to the inclined nature of the faults, the 45° between inferred maximum compressive stress and strike of the shear zone, as interpreted from map view (Fig. 9), may be smaller in reality. Moreover, set C could likewise be seen as thrust faults in the overall transpressive framework, in turn fitting our interpretation of local flower structures in other areas. Most surprising are the rather shallow dips of Set A in the eastern part of the island. Judging from their dip only suggests thrust fault kinematics of the faults. It remains difficult to determine whether these structures initiated as thrust faults and were later reactivated with strike-slip kinematics, or initial strike-slip structures have been rotated. A potential

driver for thrust faulting might be push of the Australian Plate. However, if the structures initiated as thrust faults, this would require later rotation of the stress field in such a way that the orientation of the NSFS perfectly coincides with orientation of the thrust faults of the compressive regime (i.e. rotation of $\sigma 1$ by 45°). Even though this cannot be excluded, we prefer the interpretation of later rotation of the faults and their formation within the Riedel framework. A first order test for the different hypotheses that may be carried out in the future would contain detailed field mapping of cross cutting relationships of kinematic indicators on the fault planes. In sum, we argue that the overall structural configuration of Pulau Weh Island fits within a Riedel framework, but shows partly significant complexity and deviations from a simple pattern. This potentially provides additional insights on how the strike-slip faults evolve during northwestward propagation.

The existence of Pulau Weh Island begs the question as to its cause. Within the strike-slip environment, and most importantly due to its northwestward propagation, significant amount of uplift within the sliver plate may be expected, first due to frontal and basal accretion, and secondly due to positive flower structures. Such vertical extrusion can lead to significant amount of topography, as for instance observed in the Eastern California Shear Zone (e.g. Unruh et al., 2003). As the morphology of the island is largely dominated by faults, volcanic uplift may be considered subordinate at first sight. However, the topography onshore northeast Sumatra, which is similarly fault-controlled, is clearly dominated by the Seulawah Agam active volcano. Moreover, as large-scale strike-slip faults influence the location of the volcanic arc, it cannot be excluded that at least part of the uplift is related to volcanic activity. Indeed volcanic gas emissions occur on the island (orange stars in Fig. 3). We suspect that at least partly the observed structural complexity may be caused by underlying volcanoes, as has been discussed for other areas. For instance the South Iceland Seismic Zone is a strike-slip zone that developed in close relation to the Icelandic Mantle Plume. Here, transform faulting of a relatively thin brittle layer above a hot viscous domain results in elastic response to deformation and rotation of relatively rigid blocks (Angelier et al., 2008). Another prominent example of strain partitioning and strike-slip motion within a magmatic arc is the southern Andes. Here, fault kinematic analysis shows that partly volcanoes are not structurally linked to adjacent strike-slip faults, but overall volcanic dikes and their root zones are associated with strike-slip structures such as horsetails or splays, reflecting the large scale stress field (Rosenau et al., 2006). Based on DEM analyses, the total amount of volcanic extrusion in the area has been quantified to range between 10 and 13 km3/km/Ma (Völker et al., 2011). For Sumatra, the coincidence between volcanic activity and location of the SFS has been recognized and described in several studies (e.g. McCaffrey et al., 2000, 2001; Acocella, 2014). However, as to what extend magmatic activity controls structural evolution of the SFS or vice versa remains unclear, as where in some areas the fault and volcanoes coincide, in other parts strain localization is independent of volcanic activity (Genrich et al., 2000). Our detailed analysis may provide some insights, even though untangling the ultimate cause of uplift of Pulau Weh is difficult based on our data set. The large-scale structural pattern of the island seems to reflect strike-slip movements. However, the multiple local complexities do not fit this overall pattern, which suggests volcanic activity instead. Even though the role of volcanic activity leading to strain localization should not be underestimated, the tangled interaction between volcanic activity, stress and finite strain requires exhaustive analysis and mapping (Feuillet et al., 2006; Feuillet, 2013).

5.3. The Pulau Aceh thrust splays

As opposed to Pulau Weh Island, the Pulau Aceh Archipelago does not show such a distinct Riedel pattern. Instead, the character, dip direction and dip of the planar features mapped in the archipelago let us to the interpretation of the archipelago as a train of anticlines with opening angles of consistently ~45° (Fig. 10). Such fold trains may occur in the vicinity of strike-slip zones, especially when shallow weak layers facilitate detaching of the overlying strata (e.g. Twiss and Moores, 1992)(Figs. 10 and 11). Fold trains evolve in such hybrid situations as splay contractional structures of the overall strike-slip system. The anticlines show a systematic southward decrease of the angle of their basal fault. The southernmost fault dips at an angle of 30, which is the typical angle for newly established thrust faults. Consequently we speculate that the northern fault has been rotated at a later stage, indicating southward out-of-sequence propagation of the thrusts. Such break-back sequences are common, and have been reported from various fold-and-thrust belts, for instance the European Alps (von Hagke et al., 2014b). It is noteworthy, that such fold-and-thrust belts are perpendicular to the fold-and-thrust belts, which form at the distal part of the sliver plate. This framework however requires the existence of a weak horizon within the involved sedimentary sequence, as well as predominance of the strike-slip component in the area. Such weak horizon may correspond either to the basement-cover interface or some rheological heterogeneities within the sedimentary sequence, such as the presence of deep marine shales, which are well-known décollement horizons (e.g. Rutter et al., 2013; Aydin and Engelder, 2014; Suppe, 2014). It has been shown that fluid overpressure may be an important factor; however it is not necessary for producing extremely weak shale décollement (von Hagke et al., 2014a; Morley et al., 2014). Likewise, mineralogy, amount of organic matter or structure localisation may play an important role (e.g. Rutter et al., 2013).

5.3.1. Shortening in the contractional domain

To estimate the shortening in the fold-and-thrust system of Pulau Weh, we extrapolated the bedding bulk envelop from measurements taken in outcrops, and the planar structures extracted from the DEM. Based on this bulk envelop of the bedding, we performed a restoration. As the ages of the geological formations remain poorly constrained, this restoration is only based on the geometry of the contractional system. Note that this restoration is spatially limited as we restore the deformation along the last 30 km of the NSFS. The final section length is 40 km after unfolding of the bedding. Therefore, the amount of shortening accommodated by the fold-and-thrust system in this area is ~10 km. This cross-section restoration through Pulau Aceh Archipelago allows us to give a tentative minimum shortening of 20% for the area (Fig. 10).

The geometry of the thrust splay suggests that the thrust faults root on a décollement layer at shallow depth. As 20% of deformation is accommodated in the fold-and-thrust belt, layer parallel shearing on this décollement is an important player in the overall strike-slip setting. This may be a relative important finding, as thrust systems are more likely to cause tsunami waves as opposed to strike-slip settings, which have limited tsunami hazard (Hornbach et al., 2010). Consequently quantifying the total amount of slip deficit on these structures may contribute to geohazard assessment of the area.

5.4. Stress and strain in the NSFS

Here we show that a Riedel system trending NNW–SSE and a NW-verging thrust splay system developed to the East and West of the NSFS, respectively (Figs. 11 and 12). These strain patterns were both developed under a stress field characterized by a $\sigma 1$ and $\sigma 3$ roughly trending NNE–SSW and ESE–WNW, respectively (Fernández-Blanco et al., 2015). These directions are similar to the present day principal stress axes (e.g. McCaffrey, 2009) (Figs. 12). This observation suggests a stable stress field over a certain time period that remains difficult to estimate, since the stratigraphy is poorly constrained in the area, and therefore hinders a detailed chronology of both, deposits and deformation.

Observations of the Aceh Basin suggest that the NW-verging thrust splay system of the NSFS may be a lateral step over, connecting two strike-slip fault segments that will be eventually cross-cut as the NSFS farther propagates (Berglar et al., 2010; Martin et al., 2014). Strain

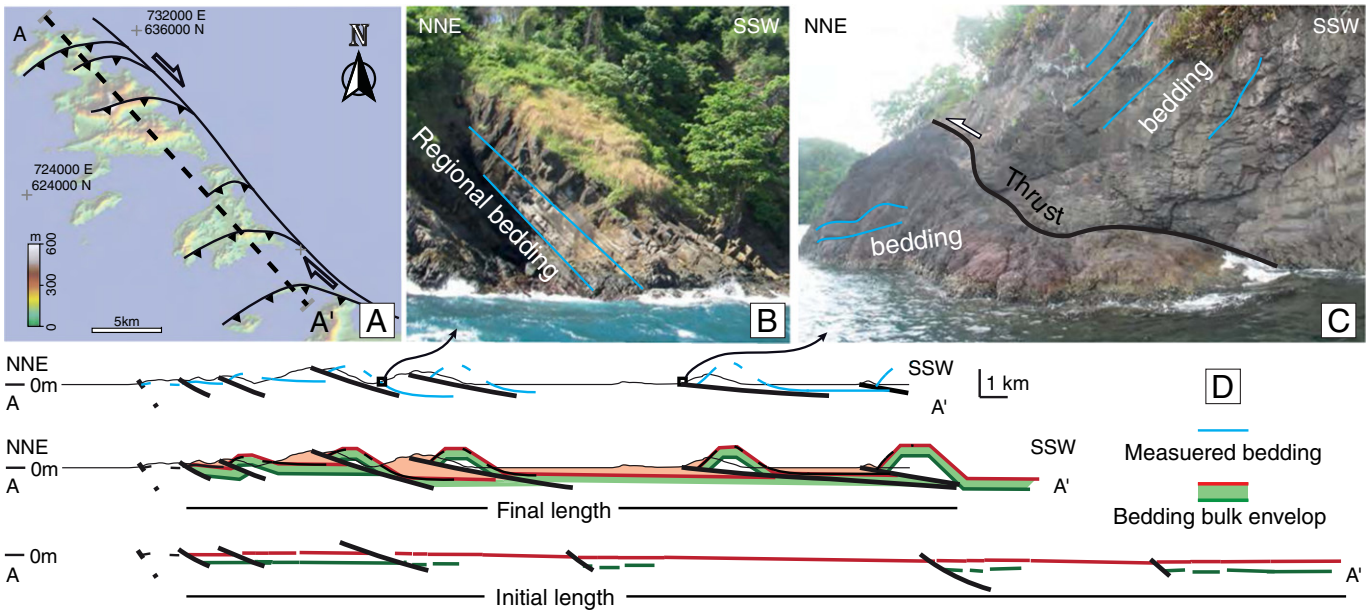

Fig. 10. Structural interpretation of the Pulau Aceh: Fold-and-thrust splays.

seems to be accommodated at present day west off Sumatra mainland, along a strike-slip fault system bounding the West of the Aceh Basin and trending parallel to the NSFS, the West Andaman Fault (WAF) (Berglar et al., 2010; Martin et al., 2014) (Fig. 1). Berglar et al. (2010) propose that the WAF has been active since the Late Miocene, and propagates northwestwardly due to oblique convergence. South of the Aceh Basin, a series of thrust faults consist in a lateral step over connecting two strike-slip faults. These faults are similar to the one we described onshore. Additionally, Martin et al. (2014) show that the WAF cross cuts former thrust faults that have initiated a the tip of a propagating strike-slip fault. Therefore, we consider possible that a similar system is developing in the NSFS area.

Moreover, mechanical models show that the tips of large-scale propagating faults develop an tensional and a compressional damage zone (e.g. Hubert-Ferrari et al., 2003). This principle was applied to explain the evolution of the Aegean as the result of the combined effect of its backarc extension in relation rollback of the Hellenic slab towards Africa (Brun and Faccenna, 2008) and the compressional damage zone developed to the south of the propagating tip of the North Anatolian Fault (Armijo et al., 2003). Similarly, our observations of the tip of the NSFS match this stress pattern, with a western compressional domain (Pulau Weh thrust splay) and an eastern tensional domain (Pulau Aceh Riedel system). However, whereas the stress pattern of the Aegean results from both fault propagation mechanics and backarc extension by

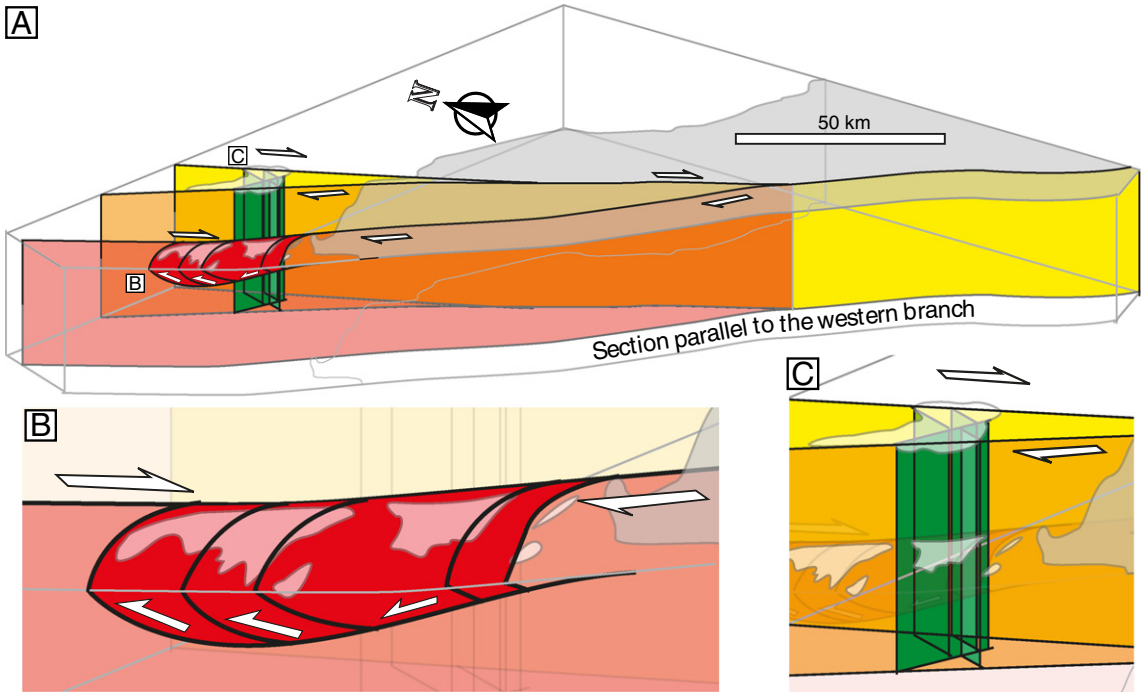

Fig. 11. 3D kinematic model for the NSFS, representing the main structures and their motion in a view parallel to its western branch. Close-up view of the fold-and-thrust system in the western branch [B] and the Riedel system in the eastern branch [C].

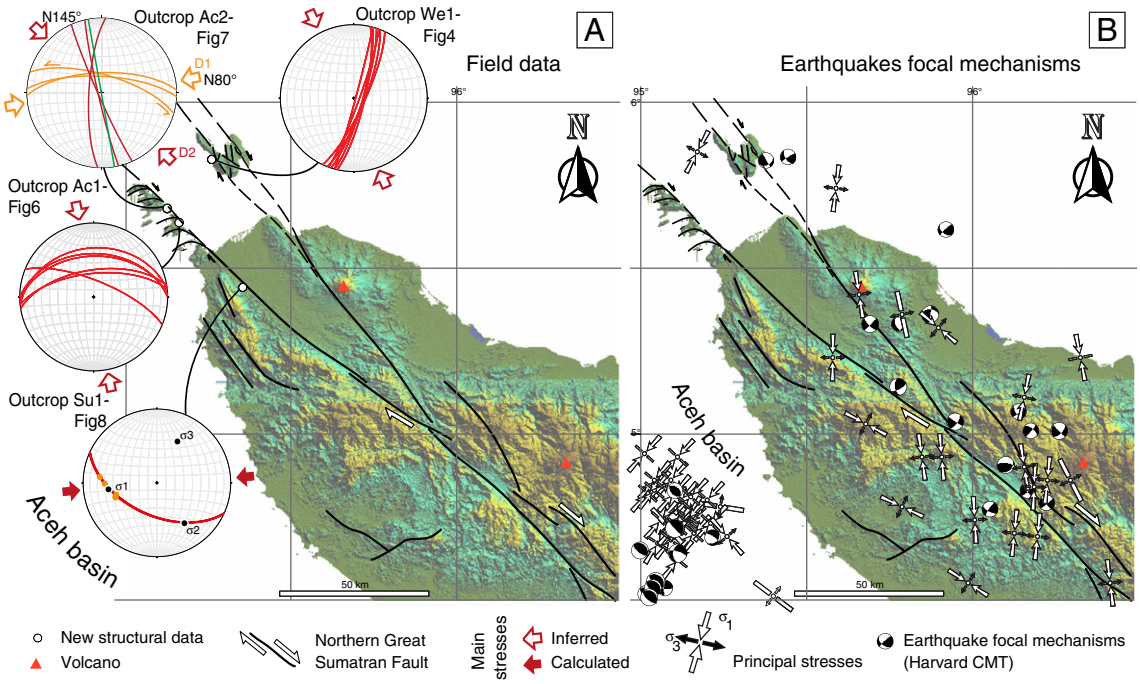

Fig. 12. A: Stereoplots showing the analysis of structural data in few selected outcrops. B: Focal mechanisms derived from earthquakes, plotted with FSA software (Célérier, 2011).

rollback, the Sunda slab is not rolling back, and thus the Sumatran backarc region is only influenced by extrusion of SE Asia in response to India-Eurasia collision (Peltzer and Taponnier, 1988). For the first time, we imaged the strain partitioning resulting from the propagation of the NSFS in Sumatra mainland (Fig. 11).

6. Conclusions

In this study we provided detailed structural analysis of the leading edge of deformation of the Sumatran Fault System, where strain is partitioned along two major fault branches. Our analysis reveals that kinematics at the exposed tip of the continental sliver features very different kinematic regimes within a relatively small area. For instance, in case of the Pulau Weh Island at the eastern branch of the NSFS, the overall structural pattern in map view represents a Riedel system. However, detailed analysis of dips of the planes in combination with uncertainty of their kinematics reveals that at least locally this big structure features complex areas, potentially related to late stage rotation of the strike-slip faults, flower structures, or transpressive thrust faults. Probably the most exciting finding of this study is the existence of a fold-and-thrust belt oriented perpendicular to the main strike direction of the large-scale strike-slip system. This secondary fold-and-thrust belt requires the existence of a weak décollement within the involved stratigraphic sequence. Importance of such weak décollement has been widely recognized in compressional settings. This study shows that they may evolve and significantly contribute to strain accommodation also in strike-slip settings, potentially related to the early stages of system evolution. This has major implications for geohazard assessment within the area; even though there are examples of strike-slip events causing tsunami (Hornbach et al., 2010), thrust faults are more likely to trigger tsunami. This study emphasizes that, in addition to GPS-based neotectonic and geophysical studies, field evidence is an essential requirement.

Acknowledgments

The authors want to thank the insightful comments and valuable input of the reviewers Sean Gulick and Juan Carlos Balanyá Roure, and to the editor, Manuel Díaz-Azpiroz. Wolfgang Straka and the project "Animal Perception of Seismic and Non-Seismic Earthquake Phenomena", funded by Red Bull Media House GmbH, made this contribution possible. D. Fernández-Blanco is indebted with Awaluddin Yusuf, Syehaffer Wahyudi, Teuku Reza and Lono Satrio for their effort on the fieldwork logistics and enjoyable company.

References

Acocella, V., 2014. Structural control on magmatism along divergent and convergent plate boundaries: overview, model, problems. Earth Sci. Rev. 136, 226–288.
Allen, C., 1965. Transcurrent faults in continental areas. R. Soc. London Phil. Trans. 258, 8289.
Angelier, J., Bergerat, F., Stefansson, R., Bellou, M., 2008. Seismotectonics of a newly formed transform zone near a hotspot: earthquake mechanisms and regional stress in the South Iceland seismic zone. Tectonophysics 447, 95–116.
Armijo, R., Flerit, F., King, G., Meyer, B., 2003. Linear elastic fracture mechanics explains the past and present evolution of the Aegean. Earth Planet. Sci. Lett. 217, 85–95.
Aydin, M.G., Engelder, T., 2014. Revisiting the Hubbert–Rubey pore pressure model for overthrust faulting: inferences from bedding-parallel detachment surfaces within Middle Devonian gas shale, the Appalachian Basin, USA. J. Struct. Geol. 69, 519–537.
Bellier, O., Sébrier, M., 1994. Relationship between tectonism and volcanism along the Great Sumatran Fault Zone deduced by SPOT image analyses. Tectonophysics 233, 215–231.
Berglar, K., Gaedicke, C., Franke, D., Ladage, S., Klingelhoefer, F., Djajadihardja, Y., 2010. Structural evolution and strike-slip tectonics off north-western Sumatra. Tectonophysics 480, 119132.
Bock, Y., Prawirodirdjo, L., Genrich, J.F., Stevens, C.W., McCaffrey, R., Subarya, C., Puntodewo, S.S.O., Calais, E., 2003. Crustal motion in Indonesia from Global Positioning System measurements. J. Geophys. Res. 108 (B8), 2367.
Brun, J., Faccenna, C., 2008. Exhumation of high-pressure rocks driven by slab rollback. Earth Planet. Sci. Lett. 272, 1–7.
Célérier, B., 2011. FSA: Fault and Stress Analysis Software, Version 33.8. Univ. Montpellier, p. 2.
Chlieh, M., Avouac, J.P., Hjorleifsdottir, V., Song, T.R.A., Ji, C., Sieh, K., Sladen, A., Hebert, H., Prawirodirdjo, L., Bock, Y., et al., 2007. Coseismic slip and afterslip of the great Mw 9.15 Sumatra–Andaman earthquake of 2004. Bull. Seismol. Soc. Am. 97, S152–S173.
Chlieh, M., Avouac, J.P., Sieh, K., Natawidjaja, D., Galetzka, J., 2008. Heterogeneous coupling of the Sumatran megathrust constrained by geodetic and paleogeodetic measurements. J. Geophys. Res. 113, B05305.
Collings, R., Lange, D., Rietbrock, A., Tilmann, F., Natawidjaja, D., Suwargadi, B., Miller, M., Saul, J., 2012. Structure and seismogenic properties of the Mentawai segment of the Sumatra subduction zone revealed by local earthquake traveltime tomography. J. Geophys. Res. 117, B01312.
Cook, B.J., Henstock, T.J., McNeill, L.C., Bull, J.M., 2014. Controls on spatial and temporal evolution of prism faulting and relationships to plate boundary slip offshore north-central Sumatra. J. Geophys. Res. Solid Earth 119, 5594–5612.

Curray, J., Moore, D., Lawver, L., Emmel, F., Raitt, R., Henry, M., Kieckhefer, R., 1979. Tectonics of the Andaman Sea and Burma: convergent margins. Am. Assoc. Pet. Geol. Bull.
Fernández-Blanco, D., Philippon, M., von Hagke, C., 2015. Present-day stress orientations in the Great Sumatran Fault in North Sumatra. Geotectonic Res. 97, 30–33.
Feuillet, N., 2013. The 20112012 unrest at Santorini rift: stress interaction between active faulting and volcanism. Geophys. Res. Lett. 40, 3532–3537.
Feuillet, N., Coco, M., Musumeci, C., Nostro, C., 2006. Stress interaction between seismic and volcanic activity at Mt Etna. Geophys. J. Int. 164, 697718.
Fitch, T., 1972. Plate convergence, transcurrent faults, and internal deformation adjacent to Southeast Asia and the western Pacific. J. Geophys. Res. 77, 44324460.
Franke, D., Schnabel, M., Ladage, S., Tappin, D.R., Neben, S., Djajadihardja, Y.S., Müller, C., Kopp, H., Gaedicke, C., 2008. The great Sumatra–Andaman earthquakesimaging the boundary between the ruptures of the great 2004 and 2005 earthquakes. Earth Planet. Sci. Lett. 269, 118–130.
Frederik, M.G.C., Gulick, S.P.S., Austin, J.A., Bangs, N.L., Udrekh, 2015. Investigation of accretionary wedge structures off north Sumatra using 2D multichannel seismic and multibeam bathymetric data. Tectonics 34. http://dx.doi.org/10.1002/2014TC003614.
Fu, G., Sun, W., 2006. Global co-seismic displacements caused by the 2004 Sumatra-Andaman earthquake (Mw 9.1). Earth Planets Space 58, 149–152.
Genrich, J., Bock, Y., McCaffrey, R., Prawirodirdjo, L., Stevens, C., Puntodewo, S., Subarya, C., Wdowinski, S., 2000. Distribution of slip at the northern Sumatran fault system. J. Geophys. Res. 105 (B12), 28,327–28,341.
Gudmundsson, Ó., Sambridge, M., 1998. A regionalized upper mantle (rum) seismic model. J. Geophys. Res. Solid Earth 103, 7121–7136.
von Hagke, C., Oncken, O., Evseev, S., 2014a. Critical taper analysis reveals lithological control of variations in detachment strength: an analysis of the Alpine basal detachment (Swiss Alps). Geochem. Geophys. Geosyst. 15, 176–191.
von Hagke, C., Oncken, O., Ortner, H., Cederbom, C., Aichholzer, S., 2014b. Late Miocene to present deformation and erosion of the central AlpsEvidence for steady state mountain building from thermokinematic data. Tectonophysics 632, 250–260.
Hatherton, T., Dickinson, W.R., 1969. The relationship between andesitic volcanism and seismicity in Indonesia, the Lesser Antilles, and other island arcs. J. Geophys. Res. 74, 530110.
Heuret, A., Lallemand, S., 2005. Plate motions, slab dynamics and back-arc deformation. Phys. Earth Planet. Inter. 149, 31–51.
Hornbach, M.J., Braudy, N., Briggs, R.W., Cormier, M.H., Davis, M.B., Diebold, J.B., Dieudonne, N., Douilly, R., Frohlich, C., Gulick, S.P., et al., 2010. High tsunami frequency as a result of combined strike-slip faulting and coastal landslides. Nat. Geosci. 3, 783–788.
Hubert-Ferrari, A., King, G., Manighetti, I., Armijo, R., Meyer, B., Tapponnier, P., 2003. Long-term elasticity in the continental lithosphere; modelling the Aden ridge propagation and the anatolian extrusion process. Geophys. J. Int. 153, 111–132.
Huchon, P., LePichon, X., 1984. Sunda Strait and central Sumatra fault. Geology 12, 668672.
Ishii, M., Shearer, P.M., Houston, H., Vidale, J.E., 2005. Extent, duration and speed of the 2004 Sumatra–Andaman earthquake imaged by the Hi-Net array. Nature 435, 933–936.
Jarrard, R., 1986. Terrain motion by strike-slip faulting of fore arc slivers. Geology 14, 780783.
Kaneko, S., 1966. Transcurrent displacement along the median line, south-western Japan. N. Z. J. Geol. Geophys. 2, 45–59.
Karig, D.E., 1978. Material transport within accretionary prisms and the "knocker" problem. J. Geol. 88, 2739.
Kasmolan, M., Santosa, B.J., Lees, J.M., Utama, W., 2010. Earthquake source parameters at the sumatran fault zone: identification of the activated fault plane. Cent. Eur. J. Geosci. 2, 455–474.
Katili, J., 1970. Large transcurrent faults in southeast Asia with spherical reference to Indonesia. Geol. Rundsch. 59, 581600.
Katili, J., Hehuwat, F., 1967. On the occurrence of large transcurrent faults in Sumatra, Indonesia. Osaka Univ. J. Geosci. 10, 5–17.
Martin, K.M., Gulick, S.P., Austin, J.A., Berglar, K., Franke, D., 2014. The West Andaman Fault: a complex strain-partitioning boundary at the seaward edge of the Aceh Basin, offshore Sumatra. Tectonics 33, 786–806.
McCaffrey, R., Wark, D., Roecker, S., Ibrahim, G., et al., 2001. Distribution of magma beneath the Toba caldera complex, north Sumatra, Indonesia, constrained by three-dimensional P wave velocities, seismicity, and gravity data. Geochem. Geophys. Geosyst. 2.
McCaffrey, R., 1991. Slip vectors and stretching of the Sumatran fore arc. Geology 19, 881–884.
McCaffrey, R., 1992. Oblique plate convergence, slip vectors, and fore arc deformation. J. Geophys. Res. 97, 89058915.
McCaffrey, R., 2009. The tectonic framework of the Sumatran subduction zone. Annu. Rev. Earth Planet. Sci. 37, 345–366.
McCaffrey, R., Zwick, P.C., Bock, Y., Prawirodirdjo, L., Genrich, J.F., Stevens, C.W., Puntodewo, S., Subarya, C., 2000. Strain partitioning during oblique plate convergence in northern Sumatra: geodetic and seismologic constraints and numerical modeling. J. Geophys. Res. 105 (28363–28).
Moreno, M., Rosenau, M., Oncken, O., 2010. 2010 Maule earthquake slip correlates with pre-seismic locking of Andean subduction zone. Nature 467, 198–202.
Morley, C.K., Warren, J., Tingay, M., Boonyasaknanon, P., Julapour, A., 2014. Comparison of modern fluid distribution, pressure and flow in sediments associated with anticlines growing in deepwater (Brunei) and continental environments (Iran). Mar. Pet. Geol. 55, 230–249.
Natawidjaja, D., Sieh, K., Chlieh, M., Galetzka, J., Suwargadi, B., Cheng, H., Edwards, R., Avouac, J.P., Ward, S., 2006. Source parameters of the great Sumatran megathrust earthquakes of 1797 and 1833 inferred from coral microatolls. J. Geophys. Res. 111, B06403.
Natawidjaja, D., Sieh, K., Ward, S., Cheng, H., Edwards, R., Galetzka, J., Suwargadi, B., 2004. Paleogeodetic records of seismic and aseismic subduction from central Sumatran microatolls, Indonesia. J. Geophys. Res. 109, B04306.
Natawidjaja, D.H., 2002. Neotectonics of the Sumatran Fault and Paleogeodesy of the Sumatran Subduction Zone (Ph.D. thesis) California Institute of Technology.
Ninkovich, D., Sparks, R., Ledbetter, M., 1978. The exceptional magnitude and intensity of the Toba eruption, Sumatra: an example of the use of deep-sea tephra layers as a geological tool. Bull. Volcanol. 41, 286–298.
Peltzer, G., Taponnier, P., 1988. Formation and evolution of strike-slip faults, rifts, and basins during the India-Asia Collision: an experimental approach. J. Geophys. Res. 93, 15085–15117.
Pesicek, J., Thurber, C., Widiyantoro, S., Engdahl, E., DeShon, H., 2008. Complex slab subduction beneath northern Sumatra. Geophys. Res. Lett. 35, L20303.
Prawirodirdjo, L., Bock, Y., Genrich, J., Puntodewo, S., Rais, J., Subarya, C., Sutisna, S., 2000. One century of tectonic deformation along the Sumatran fault from triangulation and Global Positioning System surveys. J. Geophys. Res. 105 (28), 34328–34363.
Prescott, W.H., 1981. The determination of displacement fields from geodetic data along a strike slip fault. J. Geophys. Res. Solid Earth 86, 6067–6072 (1978–2012).
Reif, D., Grasemann, B., Faber, R., 2011. Quantitative structural analysis using remote sensing data: Kurdistan, northeast Iraq. AAPG Bull. 95, 941–956.
Rosenau, M., Melnick, D., Echtler, H., 2006. Kinematic constraints on intra-arc shear and strain partitioning in the southern Andes between 38 S and 42 S latitude. Tectonics 25.
Rutter, E., Hackston, A., Yeatman, E., Brodie, K., Mecklenburgh, J., May, S., 2013. Reduction of friction on geological faults by weak-phase smearing. J. Struct. Geol. 51, 52–60.
Sieh, K., 1988. The Sunda megathrust — past, present and future. Geol. Soc. Am. Bull. 100, 1666–1703.
Sieh, K., 2007. The Sunda megathrust — past, present and future. J. Earthq. Tsunami 1, 1–19.
Sieh, K., Natawidjaja, D., 2000. Neotectonics of the Sumatran fault, Indonesia. J. Geophys. Res. 105 (28,29528,326).
Simoes, M., Avouac, J., Cattin, R., Henry, P., 2004. The Sumatra subduction zone: a case for a locked fault zone extending into the mantle. J. Geophys. Res. 109, B10402.
Simons, W., Ambrosius, B., Noomen, R., Angermann, D., Wilson, P., Becker, M., Reinhart, E., Walpersdorf, A., Vigny, C., 1999. Observing plate motions in South East Asia: geodetic results of the GEODYSSEA Project. Geophys. Res. Lett. 26, 2081–2084.
Simons, W., Socquet, A., Vigny, C., Ambrosius, B., Haji Abu, S., Promthong, C., Subarya, C., Sarsito, D., Matheussen, S., Morgan, P., et al., 2007. A decade of GPS in Southeast Asia: resolving Sundaland motion and boundaries. J. Geophys. Res. Solid Earth 112.
Socquet, A., Simons, W., Vigny, C., McCaffrey, R., Subarya, C., Sarsito, D., Ambrosius, B., Spakman, W., 2006. Neotectonics of the Sumatran fault, Indonesia. J. Geophys. Res. 111, B08409.
Subarya, C., Chlieh, M., Prawirodirdjo, L., Avouac, J.P., Bock, Y., Sieh, K., Meltzner, A.J., Natawidjaja, D.H., McCaffrey, R., 2006. Plate-boundary deformation associated with the great Aceh-Andaman earthquake. Nature 440, 46–51.
Suppe, J., 2014. Fluid overpressures and strength of the sedimentary upper crust. J. Struct. Geol. 69, 481–492.
Twiss, R.J., Moores, E.M., 1992. Structural Geology. Macmillan.
Unruh, J., Humphrey, J., Barron, A., 2003. Transtensional model for the Sierra Nevada frontal fault system, eastern California. Geology 31, 327–330.
Völker, D., Kutterolf, S., Wehrmann, H., 2011. Comparative mass balance of volcanic edifices at the southern volcanic zone of the Andes between 33 S and 46 S. J. Volcanol. Geotherm. Res. 205, 114–129.
Walter, T.R., Amelung, F., 2007. Volcanic eruptions following M 9 megathrust earthquakes: implications for the Sumatra-Andaman volcanoes. Geology 35, 539–542.